Supporting Information

InGaN/GaN multi-quantum well LED array for short distance optical links

Xueyao Lu[1], Xumin Gao[1], Xiaoxuan Wang[3]*, Yang Chen[1], Xin Li[1], Fan Shi[1], Fang Liu[4], Xu Wang[2]*, Feifei Qin[1]* and Yongjin Wang[1]*

[1]*GaN Optoelectronic Integration International Cooperation Joint Laboratory of Jiangsu Province, Nanjing University of Posts and Telecommunications, Nanjing, 210003, China.*

[2]*Department of Microelectronic Science and Engineering, School of Physical Science and Technology, Ningbo University, Ningbo 315211, China.*
[3]*State Key Laboratory of Digital Medical Engineering, School of Electronic Science and Engineering, Southeast University, Nanjing 210096, China.*
[4]*Beijing Key Laboratory of Passive Safety Technology for Nuclear Energy, School of Nuclear Science and Engineering, North China Electric Power University, Beijing, 102206, China.*

*Corresponding authors: *qinfeifei@njupt.edu.cn (Feifei Qin)*
wangxu1@nbu.edu.cn (Xu Wang)
wangyj@njupt.edu.cn (Yongjin Wang)
wxxseu@seu.edu.cn (Xiaoxuan Wang)

A. Characterization of the optoelectronics, morphology and communication performance of LED devices

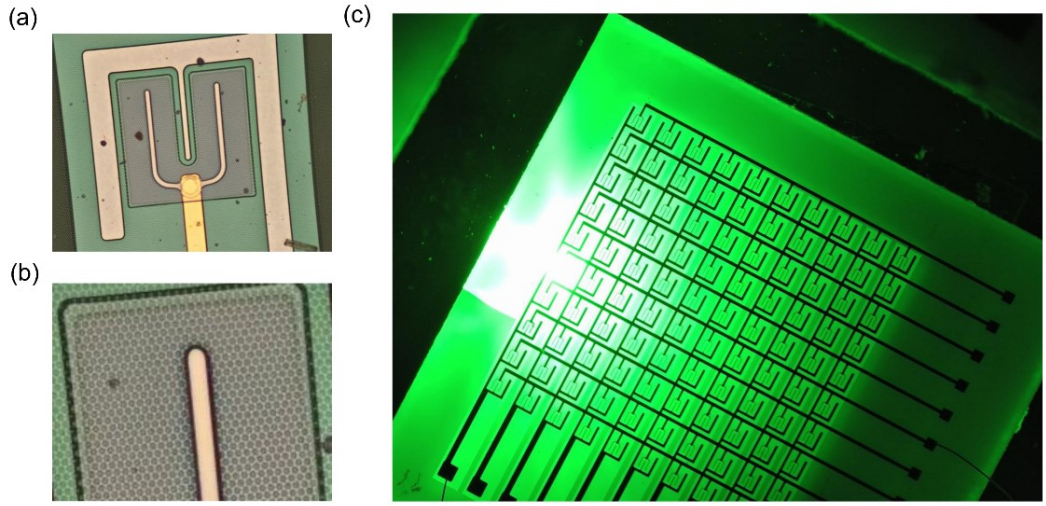

Fig. S1. (a) CCD image of an individual LED, (b) Enlarged CCD image of individual LED, (c) GaN LED array at work state.

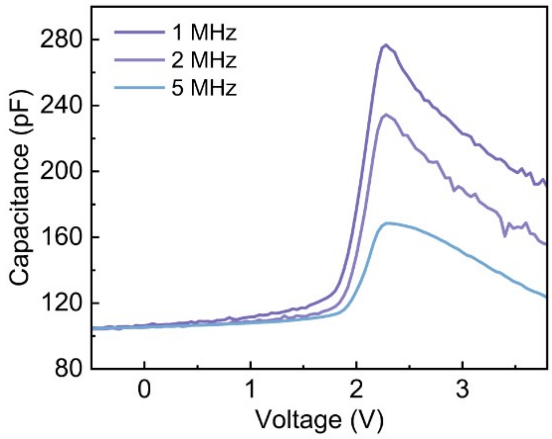

Fig. S2. C-V characteristics of the detector.

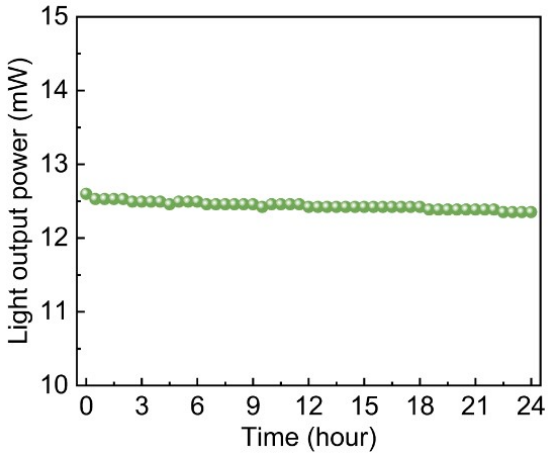

Fig. S3. Long-term power stability test results.

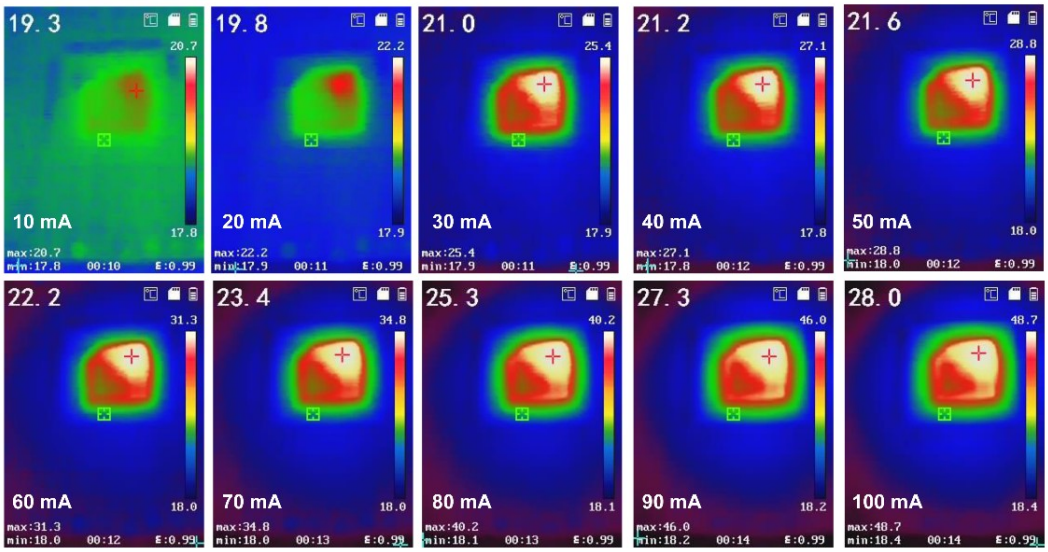

Fig. S4. Thermal imaging of the chip array under different driving currents.

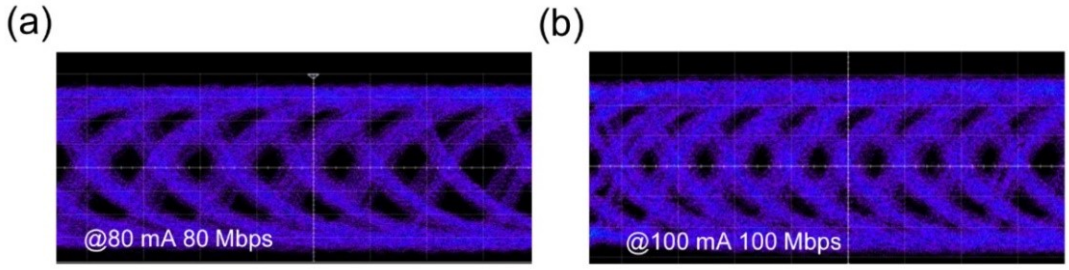

Fig. S5. Eye diagrams of individual LED under different bias current and data rate. (a) 80 mA-80 Mbps. (b) 100 mA-100 Mbps.

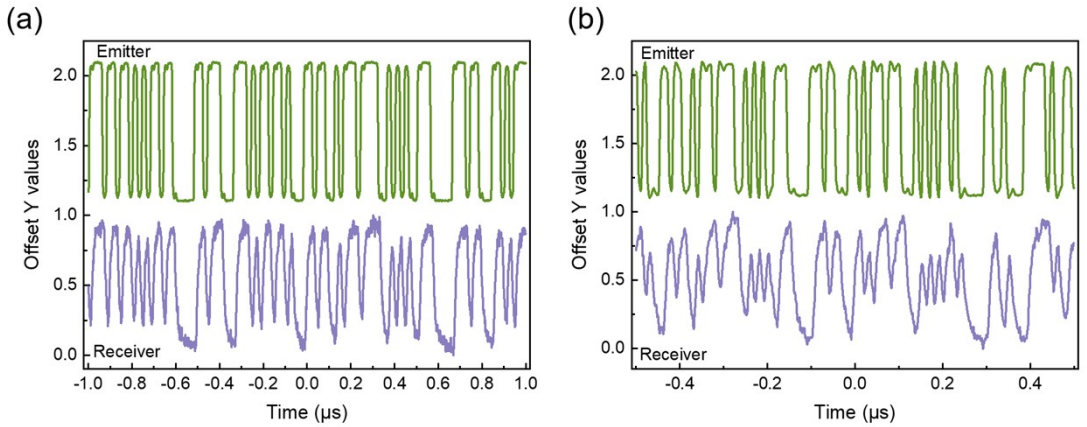

Fig. S6. The PRBS signal of data transmission at (a) 70 mA-50 Mbps and (b) 70 mA-100 Mbps.

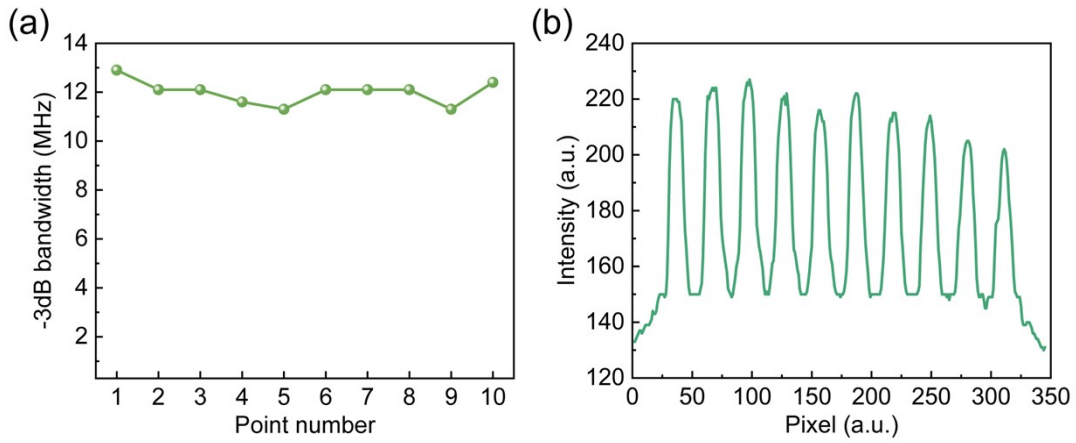

Fig. S7. (a) bandwidth summary of 10 points at one row. (b) Signal strength scan.

B. Design and realization of the audio and video communication system

Since the communication units enable a total chip data rate exceeding 500 Mbps, sufficient for typical applications such as serial communication and audio/video transmission. For context, standard UART operates at tens to hundreds of kbps, while low-data-rate audio requires several hundred kbps to ~1 Mbps, making the demonstrated per-channel rate of ~50 Mbps adequate for these scenarios. As an example, we design and built an audio and video communication. As shown in Fig. S8a, the video and audio signals are modulated through a circuit, and spectrum shifting technology separates signals in different frequency bands, preventing interference between them. The original signals are obtained at the receiving end through a demodulation circuit.

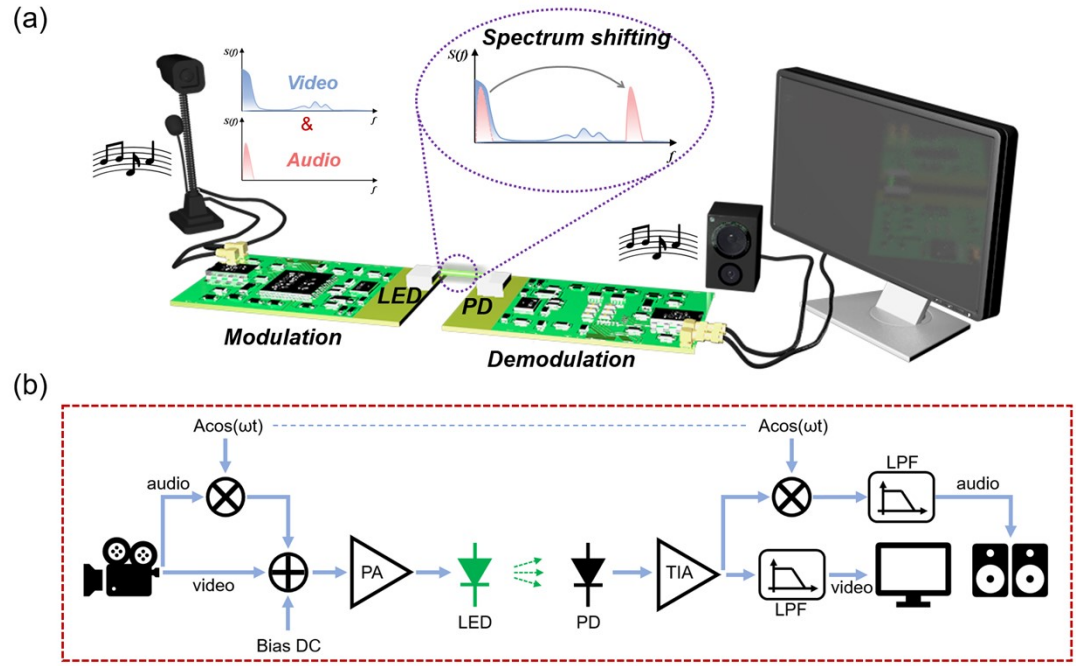

Fig. S8. (a) The concept of using a single InGaN/GaN LED to simultaneously transmit video and audio signals, the audio signal is separated from the video signal spectrum through spectral shifting, preventing aliasing during transmission. (b) Block diagram of an audio-video simultaneous transmission system.

The design in Fig.8a requires a high-speed light source and subsequent circuitry support. The single-channel data transmission capacity of over 50 Mbps ensures the bandwidth requirements. As for the subsequent circuitry support, as shown in Fig.S8b, in the experiment, a PAL-format video signal output from an analogue camera and an audio signal were selected as signal sources, using a carrier modulation signal processing method: at the transmitting end, the audio signal is modulated to a high-frequency band and then added to the video signal for joint transmission to the receiving end. At the receiving end, the original audio and video signals are recovered using coherent demodulation technology.

From a mathematical perspective, the signal processing process at the modulation end can be represented as

$$s(t) = m(t) \cdot c(t) + g(t) \#(1)$$

$m(t)$ is the audio signal, $g(t)$ is the video signal. $c(t)$ is the carrier signal, which is usually a high-frequency sine wave, represented as

$$c(t) = Acos(2\pi ft) \#(2)$$

A is the amplitude of the carrier, and f is the frequency of the carrier. By substituting $c(t)$ into $s(t)$, we obtain the modulated signal as

$$s(t) = m(t) \cdot Acos(2\pi ft) + g(t) \#(3)$$

When the signal reaches the receiving end, the received signal $s(t)$ will be processed by a demodulator to recover the original audio signal $m(t)$ and video signal $g(t)$. Specifically, the video signal can be obtained directly through low-pass filtering.

In the coherent demodulation process, the received signal $s(t)$ is mixed with the locally generated carrier signal $c_{loc}(t)$

$$s_{mix}(t) = s(t) \cdot c_{loc}(t) = m(t) \cdot Acos(2\pi ft) \cdot A_{loc}cos(2\pi ft) + g(t) \cdot A_{loc}cos(2\pi ft) \quad (4)$$

According to the trigonometric identities

$$cos^2(2\pi ft) = \frac{1 + \cos(4\pi ft)}{2} \#(5)$$

$s_{mix}(t)$ will be express as:

$$s_{mix}(t) = m(t) \cdot A \cdot A_{loc} \cdot \frac{1 + \cos(4\pi ft)}{2} + g(t) \cdot A_{loc}cos(2\pi ft) \#(6)$$

Next, by using a low-pass filter to remove the high-frequency components $\cos(4\pi ft)$ and $cos(2\pi ft)$, we can obtain the audio signal

$$m_{out}(t) = m(t) \cdot A \cdot \frac{A_{loc}}{2} \#(7)$$

Based on the data derivation process in Eq.1-7, a matching circuit was designed to achieve the superposition and transmission of the two signals. Fig. S9a and b show the specific implementation of the transmitter and receiver circuits. At the transmitter end, an AD835 analog multiplier from ADI is used to construct the amplitude modulation (AM) circuit module, enabling the modulation of the audio

baseband signal with an 8 MHz carrier signal, thereby transferring the signal spectrum to the carrier band. The modulated RF signal is processed by an in-phase summing circuit based on a high-speed operational amplifier, in which the voltage gain is set by a feedback resistor network; adjusting the resistor values allows continuous gain control from 0 to 10 dB, meeting signal strength requirements for different transmission distances. A 2.5 V DC bias is also added to precisely match the signal's DC component with the LED's optimal operating point. The final driver stage uses a TI OPA2673 high-speed, high-current operational amplifier to construct an in-phase amplifier circuit, with a maximum output current of 400 mA, ensuring high-fidelity electro-optical conversion of the composite signal.

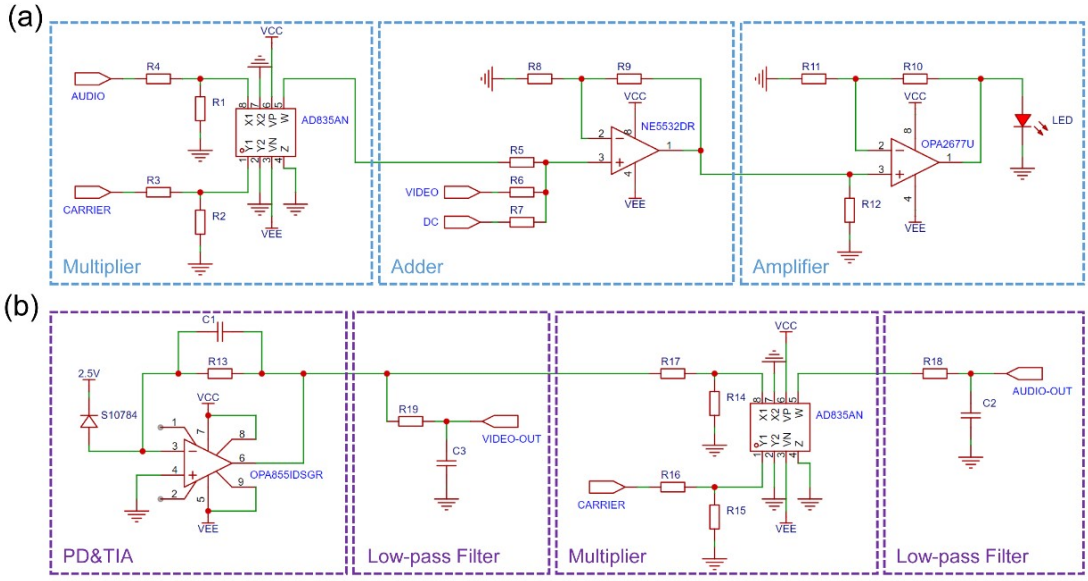

Fig. S9. (a) Transmitter circuit diagram. (b) Receiver circuit diagram.

At the receiver end, a Hamamatsu S10784 PIN photodiode (responsivity 0.45 A/W@650 nm, junction capacitance 4.5 pF, cut-off frequency 250 MHz) serves as the core photo conversion component, paired with a TI OPA855 ultra-broadband operational amplifier (gain-bandwidth product 8 GHz) to build a trans impedance amplifier (TIA). By optimizing the feedback network parameters, a trans impedance gain of 20 kΩ is achieved while maintaining an -3 dB bandwidth of 80 MHz, ensuring high-precision voltage conversion of the photocurrent. The signal demodulation module employs two processing paths: one path directly recovers the video baseband signal through a 6 MHz RC low-pass filter; the second path uses coherent detection, mixing the residual RF signal with a locally regenerated carrier, then passing through a 10 kHz RC low-pass filter to eliminate high-frequency harmonics, ultimately reconstructing the audio signal.

Fig. S10(a) and (b) show the time-domain waveforms and spectra of video signals at each key node, respectively. From the time-domain waveforms, it can be seen that the original video signal does not exhibit significant distortion after modulation, and the received signal is almost identical to the original signal, with only slight frequency distortion. In the frequency domain, it is clearly seen that the video

signal's frequency mainly lies within 6 MHz, while the audio signal has been successfully modulated to 8 MHz, which is completely consistent with our design expectations, demonstrating the accuracy and effectiveness of the modulation process. Fig. S10(c) and (d) show the original and demodulated audio signals and their spectra. From the time-domain waveforms, it can be observed that the demodulated audio signal only has a reduced amplitude compared with the original signal, with no obvious distortion in the envelope. From the spectra, it is clear that the demodulated audio signal's spectrum matches the characteristics of the original audio signal, indicating that the audio signal has been well preserved during transmission, with no significant spectral distortion or signal loss.

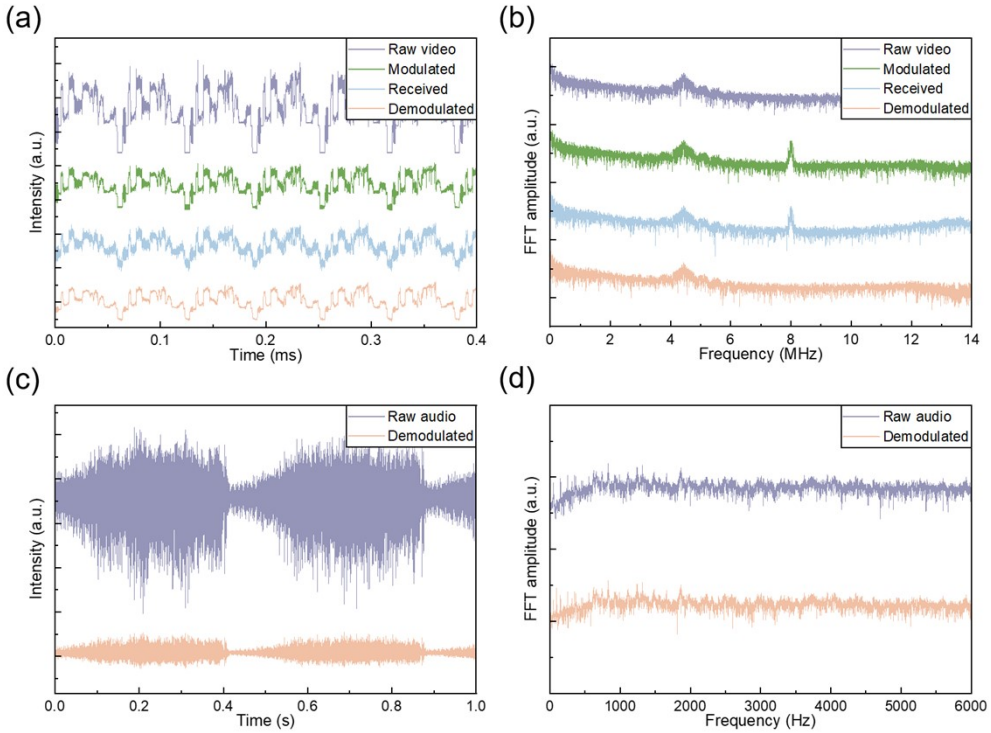

Fig. S10. Time-domain and frequency-domain waveforms at each node. (a)-(b) Time-domain and frequency-domain waveforms of the video signal; (c)-(d) Time-domain and frequency-domain waveforms of the audio signal.

C. Description for video presentation

To further illustrate the audio-video communication system, we have shot a video which provides a detailed explanation as follows：The working status of the entire system can be seen in the video support file. The camera is fixed on the left side, shooting a doll, and there is a mobile phone playing music beside the camera. The middle parts are respectively the modulation circuit and the demodulation circuit, as well as the LED and PD. The signal generator is used to provide carrier signals. When the doll on the left is shaken, the display on the right synchronously shows the shaking image, and the music played by the mobile phone on the left is transmitted in real time to the speaker on the right. As the camera moves, the music from the mobile phone on the left and the speaker on the right can be clearly heard respectively.